Nonlinear dynamics of a model for parallel pumping in ferromagnets

G. Broggi, P. F. Meier, and R. Stoop
Physik Institut der Universität Zürich, Schönberggasse 9, CH-8001 Zurich, Switzerland

R. Badii
Institut für Theoretische Physik der Universität Zürich, Schönberggasse 9, CH-8001 Zurich, Switzerland
(Received 28 April 1986)

The dynamics of a model, which has recently been proposed to simulate parallel pumping experiments in ferromagnets, has been investigated. With increasing pumping amplitude the system displays periodic, quasiperiodic, and chaotic motion. In addition, the influence of noise at a particular transition point is discussed in connection with the experimental results.

I. INTRODUCTION

Early experiments[1] on spin-wave parametric pumping in magnetically ordered samples have shown that turbulent behavior of the response signals may occur if the rf driving field exceeds a critical value. The theoretical explanation of these phenomena by Suhl[2] was based on the nonlinear coupling between the uniform precession mode of the magnetization and spin-wave modes.

The recent general interest in nonlinear phenomena has led to several new experiments[3–6] in ferromagnetic resonance and to interpretations[7,8] of the results in the context of the theory of dynamical systems.[9] The basic dynamical variable is the precessing uniform magnetization $M(t)$ of the ferromagnetic sample and the control parameter is the strength of the pumping field. Gibson and Jeffries[4] observed chaotic dynamics in gallium-doped yttrium iron garnet under transverse pumping whereas different scenarios were found[3,5,6] in longitudinal pumping experiments. Various models were suggested[4,6–8] which partially reproduce some of the observations.

To explain the irregular time sequences of spikes observed in their parallel pumping experiments, Waldner *et al.*[10–11] have recently proposed a model which simulates the behavior of the uniform magnetization with an additional interaction with the microwave cavity. The cavity is described as a damped LC circuit. In the present contribution, the results of a more detailed study of this model are given and the modalities of the transitions to chaos upon increasing the pumping strength are investigated.

In Sec. II the model is described. The equations of motion are then rescaled and a stability analysis is performed. In Sec. III the solutions are investigated in terms of properties of Poincaré sections. The influence of noise, which is crucial for a discussion of multistability and which can explain the occurrence of relaxation oscillations, is discussed in Sec. IV.

II. MODEL

The starting point of Waldner *et al.*[10] is the Landau-Lifshitz equation for the homogeneous magnetization $\mathbf{M}$ of the ferromagnetic sample

$$\frac{d\mathbf{M}}{dt}=\mathbf{M}\times\mathbf{h}-\lambda\mathbf{M}\times(\mathbf{M}\times\mathbf{h}) , \tag{1}$$

where $\mathbf{M}$ is assumed to be normalized ($|\mathbf{M}|=1$), λ is the Landau-Lifshitz damping constant, and $\mathbf{h}=\gamma\mathbf{H}$, with γ being the gyromagnetic ratio and $\mathbf{H}$ the magnetic field. The contributions to the effective field $\mathbf{h}$ are given by

$$\mathbf{h}=\mathbf{h}_0+\mathbf{h}_A+\mathbf{h}_p+\mathbf{h}_c , \tag{2}$$

where $\mathbf{h}_0$ denotes the static external field directed along the z axis, $\mathbf{h}_A$ stands for the anisotropy field, $\mathbf{h}_p$ is the pumping field, and $\mathbf{h}_c$ is the cavity field. For an anisotropy energy with hard x axis and easy y-z plane, the components of $\mathbf{h}_0$ and $\mathbf{h}_A$ are

$$\mathbf{h}_0=(0,0,h_0) \text{ and } \mathbf{h}_A=(-d_A M_x,0,0) , \tag{3}$$

with $d_A>0$ denoting the anisotropy constant. The parallel pumping term with amplitude F and frequency ω_p can be written as $\mathbf{h}_p=F\sin(\omega_p t)\mathbf{h}_0$.

The essential modification to the Landau-Lifshitz model is the introduction of an interaction with an LC circuit, whose coil has the axis along the z direction. This introduces two additional dynamical variables: the cavity field $\mathbf{h}_c=(0,0,h_c)$, and b, which is proportional to the charge on the capacitor. The corresponding Kirchhoff equations are given by

$$\begin{aligned}\frac{dh_c}{dt}&=-\gamma_c h_c-\omega_c^2 b-B_M\frac{dM_z}{dt}-B_p\frac{dh_p}{dt} ,\\ \frac{db}{dt}&=-\gamma_b b+h_c ,\end{aligned} \tag{4}$$

where γ_c and γ_b are damping parameters, B_M and B_p denote the couplings, and ω_c is the cavity frequency.

Since $|\mathbf{M}|=1$, the dynamics of $\mathbf{M}$ is conveniently described in terms of the polar and azimuthal angles θ and ϕ, which are defined by

$$\mathbf{M}=(\sin\theta\cos(\phi/2),\sin\theta\sin(\phi/2),\cos\theta) .$$

It is also convenient to introduce the variables $\alpha(t)=h_c(t)/h_0$ and $\beta(t)=b(t)d_A/h_0$ and rescale the time t to $t'=d_A t$, such that $\omega=\omega_p/d_A$ is the dimensionless frequency. By considering the rescaled field

$$\mathbf{H}=-M_x\mathbf{e}_x+H_0[1+F\sin(\omega t')+\alpha]\mathbf{e}_z$$

and the parameters $H_0=h_0/d_A$, $\gamma_\alpha=\gamma_c/d_A$, $\gamma_\beta=\gamma_b/d_A$, $g_\beta=(\omega_c/d_A)^2$, and $B_q=B_M/h_0$, the equations of motion are finally transformed into

$$\begin{aligned}
\frac{d\phi}{dt}&=-(1+\cos\phi)\cos\theta+\lambda\sin\phi-2H_0[1+F\sin(\omega t)+\alpha]\ ,\\
\frac{d\theta}{dt}&=-\tfrac{1}{2}\sin\theta\left[(1+\lambda^2)\sin\phi-\lambda\frac{d\phi}{dt}\right]\ ,\\
\frac{d\alpha}{dt}&=-\gamma_\alpha\alpha-g_\beta\beta-B_p\omega F\cos(\omega t)+B_q\sin\theta\frac{d\theta}{dt}\ ,\\
\frac{d\beta}{dt}&=-\gamma_\beta\beta+\alpha\ ,
\end{aligned}\tag{5}$$

where we have indicated again the rescaled time t' with t.

The dynamics of this five-dimensional system (four variables plus a forcing term) exhibits a variety of different behaviors as will be discussed in Sec. III where the dependence on the pumping amplitude F is investigated. The values of the other parameters, which have been kept fixed, were chosen according to Ref. 10 and are given in Table I.

In the absence of the pumping term the fixed points of the model are determined by $\alpha=\beta=0$ and $\mathbf{M}\times\mathbf{H}=\mathbf{0}$. This latter condition can be satisfied either by $\mathbf{M}=(\pm(1-H_0^2)^{1/2},0,-H_0)$ or by

$$\mathbf{M}=(0,0,\pm1)\ .\tag{6}$$

In accordance with Ref. 10 only the case $H_0>1$ will be considered. Then only the two fixed points given by Eq. (6) exist. It is easy to show that the upper one (north pole, $\theta=0$) is stable.

Three frequencies characterize the time behavior of the system: (i) the Larmor precession frequency ω_L which for small polar angles θ is $\omega_L=[h_0(h_0+d_A)]^{1/2}$ or in rescaled form $\omega_L'=[H_0(H_0+1)]^{1/2}$; (ii) the pump frequency ω_p which is kept fixed near the value $2\omega_L$, and (iii) the resonance frequency ω_c of the cavity which is incommensurate with respect to ω_L and ω_p. Therefore one expects in general the system to exhibit either periodic or quasiperiodic solutions with at most two incommensurate frequencies (two tori).

III. ANALYSIS OF THE SOLUTIONS

The system equations (5) have been integrated numerically and the solutions have been analyzed by projecting the four-dimensional Poincaré section either onto the M_x-M_y plane or onto the θ-ϕ plane. Sections were taken at intervals of a period of the forcing term $T=2\pi/\omega$ and the integration steps were chosen around $T/50$. As an example, we show in Fig. 1 the M_x-M_y representation of the trajectories for various values of F. A schematic overview of the behavior of the solutions as a function of F is displayed in Fig. 2.

For small pumping amplitude ($F<F_0$), the stable fixed point of the unperturbed system [i.e., the north pole $\mathbf{M}=(0,0,1)$] becomes a limit cycle of period 1, where the magnetization precesses with the same period as the forcing term. This corresponds in Fig. 2 to the segment marked with LC. In the projection of Fig. 1(a), one obtains a single dot at the origin. At $F=F_0$, this limit cycle becomes unstable and the system undergoes a Hopf bifurcation yielding a torus, which is indicated by T_0 in Fig. 2. If the motion is on a torus, it appears as a closed curve in the Poincaré map [see Fig. 1(a)]. One of the two frequencies characterizing the torus is ω, the other one being the frequency of circulation along the path in the Poincaré map. The diameter of T_0 becomes larger as F is increased, until the torus collides with the unstable limit cycle [Fig. 1(b)] for $F=F_1$. At this point, T_0 transforms into a new torus (labeled by T_1 in Fig. 2) which encloses the north pole $\theta=0$. The corresponding motion in the projection is displayed in Fig. 1(c). A further increase in the control parameter F yields morphological changes in the structure of T_1 which evolves through an alternation of periodic and quasiperiodic motions until chaos is first reached at a value $F=F_c\simeq1.45$. For still higher F values, the chaotic attractor (shaded in Fig. 2) enlarges until it covers the whole unit sphere. As an example the chaotic solution at $F=1.5$ is shown in Fig. 1(d).

TABLE I. Values of the dimensionless parameters used in Eq. (5).

$H_0=\frac{8.5}{3}$
$\omega=\frac{20}{3}$
$\lambda=0.01$
$\gamma_\alpha=1.909\,859\,317\times10^{-3}$
$\gamma_\beta=100\gamma_\alpha$
$g_\beta=3.61$
$B_p=0.288$
$B_q=2.340\,513\,868$

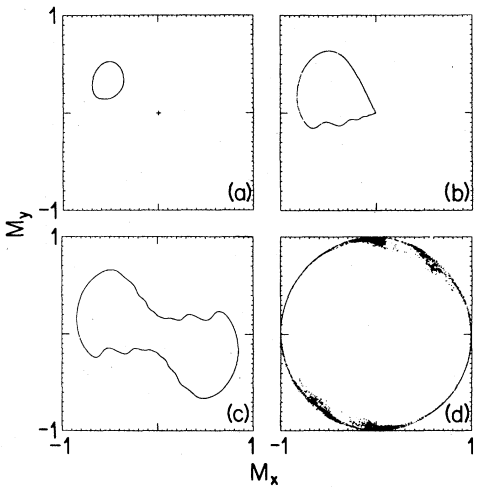

FIG. 1 Projection of the second iterate of the Poincaré section onto the M_x-M_y plane. The figures show the solutions corresponding to different pumping amplitudes F. (a) limit cycle LC (small cross) for $F=1.1$ displayed together with torus T_0 (closed curve), plotted for $F=1.2$; (b) torus T_0 at the collision with the unstable limit cycle LC ($F=1.315$); (c) torus T_1 at $F=1.4$; (d) chaotic solution after the disappearance of torus T_1 ($F=1.5$).

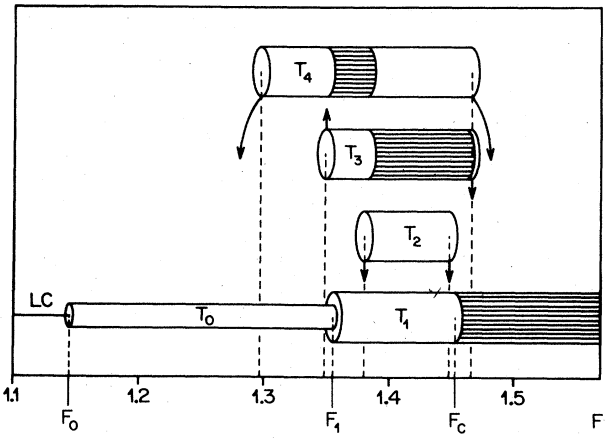

FIG. 2. Schematic representation of the regions of existence of solutions vs the pumping parameter F. The straight line marked with LC represents the small-amplitude limit cycle. Each of the cylinders shows the region of existence of a torus. In the case in which different solutions exist simultaneously arrows indicate the observed transient evolutions. Shaded areas represent the main chaotic regions.

By changing the initial conditions it has been found that three other tori (T_2, T_3, and T_4) coexist with T_0 or T_1 for some F values (see Fig. 2). They appear after a tangent bifurcation (i.e., they disappear by intermittency if F is decreased). Their evolution is very similar to that of T_1 with the exception of T_2 on which no chaotic behavior has been found. Notice that on tori T_3 and T_4 chaos occurs for smaller F values than on T_1. This seems to be a peculiarity of the model, since usually one expects chaos to originate from a structure evolving continuously from zero amplitude. In Fig. 2, the regions of existence of the five tori are shown, together with the observed transitions indicated by arrows.

Figure 3 depicts the torus T_3 at $F=1.456$, i.e., in the chaotic region. The projection of torus T_4 for $F=1.33$ is shown in Fig. 4 as an example of a fractal torus. Such quasiperiodic solutions are obtained in our system due to the presence of the characteristic frequencies ω_L and ω_c, at variance with the models discussed in Refs. 6—8 where period doublings have been found. The reconstruction of these structures from experimental data by utilizing embedding techniques allows the measurement of dynamical invariants like Lyapunov exponents, metric entropies, and fractal dimensions.[9]

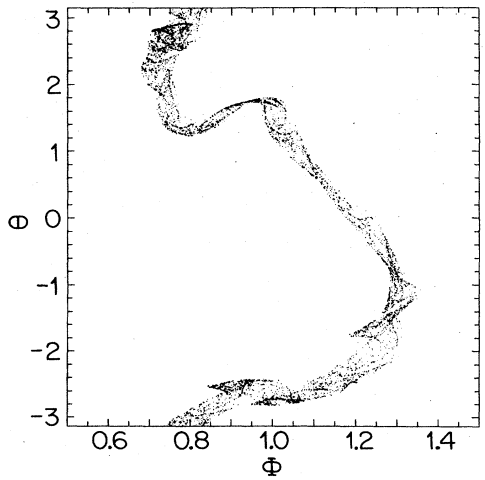

FIG. 3. Projection of the Poincaré section onto the θ-ϕ plane which displays torus T_3 (see Fig. 2) at $F=1.456$ (chaotic region).

As is well known (see, e.g., Refs. 9 or 12), the transition from quasiperiodicity to chaos can occur in several different ways. In our system, we essentially observe amplitude instabilities (fractal tori) and phase instabilities. In Sec. IV we make a connection between the experimental observations and the numerical simulations in the vicinity of the transition from T_0 to T_1.

IV. INFLUENCE OF NOISE

In Ref. 10 the authors reported the observation of "relaxation oscillations" and transitions to chaos characterized by spikes irregularly spaced in time but with nearly constant amplitude. This is a typical intermittent behavior which cannot be straightforwardly interpreted within the framework of quasiperiodic transitions. Since a description of this phenomenon could not be obtained using deterministic equations only, we took into account the presence of noise. Fluctuations probably also inhibit the experimental observation of the multistability found in the numerical solutions. Indeed, experimentally only the route to chaos following the LC-T_0-T_1 sequence has so far been detected.

To simulate the influence of fluctuations a numerical integration of Eqs. (5) has been performed by including an additive Gaussian white noise with amplitude q in the resonator equation for the variable α. As an example of the solutions the time evolution of the longitudinal magnetization M_z for $F=1.351\,48$ (i.e., F slightly larger than F_1) and $q=10^{-6}$ is shown in Fig. 5. The simulations exhibit a good qualitative agreement with the experimental observations. The appearance of spikes separated by quiescent phases is mainly due to the slowing down occur-

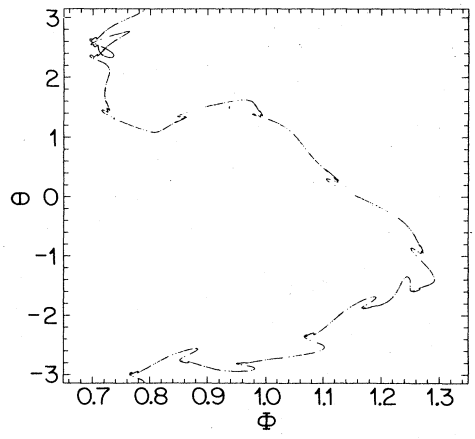

FIG. 4. Same as in Fig. 3 for torus T_4 at $F=1.33$ showing the occurrence of a fractal structure.

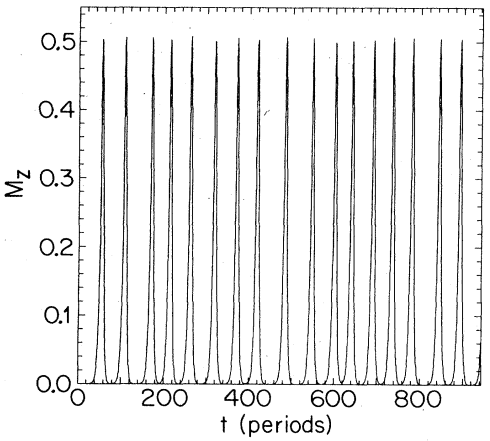

FIG. 5. Time evolution of longitudinal magnetization M_z for fluctuation amplitude $q=10^{-6}$ and $F=1.351\,48$ displaying wide plateaus separating spikes of nearly constant amplitude.

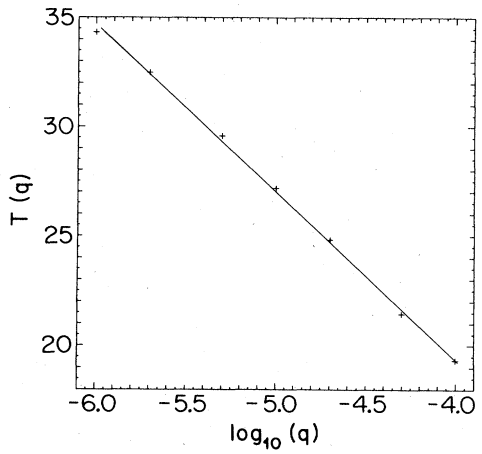

FIG. 6. Average duration $T(q)$ of the quiescent phases vs the logarithm of the noise amplitude q, calculated for $F=1.351\,48$.

ring in the neighborhood of the unstable limit cycle LC, where the presence of noise can sensitively affect the length of the plateaus. To characterize this phenomenon the average time $T(q)$ spent within a small distance ($\sim 10^{-2}$) from the north pole was calculated as a function of the noise amplitude q. In Fig. 6 $T(q)$ is plotted versus the logarithm of the fluctuation amplitude q. It is seen that the dwelling time in the vicinity of the north pole scales as $T(q)\sim \log_{10}(1/q)$. The same behavior is observed for a finite range of F values. This anomalous behavior which is caused by the combination of slowed-down deterministic motion and noise, resembles that of bistable systems close to threshold,[13] and in fact differs from the usual law $T(q)\sim 1/\sqrt{q}$ occurring in ordinary intermittency.[14] In connection with these theoretical predictions a careful experimental investigation of the controlled influence of noise on the dynamic behavior of the system would be of value and interest.

V. CONCLUSIONS

The model proposed in Ref. 10 to simulate the parallel pumping in a ferromagnetic sample with crystalline anisotropy has shown, upon an extensive numerical investigation, a very rich dynamical behavior. An overview of the phenomena which the system displays has been given in Fig. 2, where the various solutions are represented as a function of the pumping amplitude F. The model shows multistability, and on tori T_3 and T_4 chaos was found to occur for smaller F values than on T_1. It has been shown that the influence of noise is crucial for the time evolution of the system in the neighborhood of the unstable limit cycle.

Extensions of the model to account for perpendicular pumping or to investigate the interaction of several spin-wave modes[10] are feasible.

In conclusion, it seems that the turbulent behavior observed in spin-wave parametric-pumping experiments in magnetically ordered samples offers new possibilities to study, both experimentally and theoretically, a variety of quasiperiodic transitions to chaos.

ACKNOWLEDGMENTS

The authors wish to thank F. Waldner for encouraging interest and valuable help. This work has been supported by the Swiss National Science Foundation.

[1]R. W. Damon, Rev. Mod. Phys. **25**, 239 (1953); N. Bloembergen and S. Wang, Phys. Rev. **93**, 72 (1954); T. S. Hartwick, E. R. Peressini, and M. T. Weiss, J. Appl. Phys. **32**, 223S (1961).

[2]H. Suhl, Proc. IRE **44**, 1270 (1956); J. Phys. Chem. Solids **1**, 209 (1957).

[3]H. Yamazaki, J. Phys. Soc. Jpn. **53**, 1155 (1984).

[4]G. Gibson and C. Jeffries, Phys. Rev. A **29**, 811 (1984).

[5]D. R. Barberis, F. Waldner, and H. Yamazaki, in *Proceedings of the* XXII *Congress AMPERE on Magnetic Resonance and Related Phenomena, Zurich,* edited by K. A. Müller, R. Kind, and J. Roos (Zurich Ampere Committee, University of Zurich, Zurich, 1984), pp. 149 and 150.

[6]S. M. Rezende, F. M. de Aguiar, and O. F. de Alcantara Bonfim, J. Magn. Magn. Mater. **54—57**, 1127 (1986); F. M. de Aguiar and S. M. Rezende, Phys. Rev. Lett. **56**, 1070 (1986).

[7]K. Nakamura, S. Ohta, and K. Kawasaki, J. Phys. C **15**, L143 (1982).

[8]X. Y. Zhang and H. Suhl, Phys. Rev. A **32**, 2530 (1985).

[9]J. P. Eckmann and D. Ruelle, Rev. Mod. Phys. **57**, 617 (1985).

[10]F. Waldner, D. R. Barberis, and H. Yamazaki, Phys. Rev. A **31**, 420 (1985).

[11]F. Waldner, R. Badii, D. R. Barberis, G. Broggi, W. Flöder, P. F. Meier, R. Stoop, M. Warden, and H. Yamazaki, J. Magn. Magn. Mater. **54—57**, 1135 (1986).

[12]K. Kaneko, *Collapse of Tori and Genesis of Chaos in Dissipative Systems* (World Scientific, Singapore, 1986).

[13]G. Broggi, L. A. Lugiato, and A. Colombo, Phys. Rev. A **32**, 2803 (1985).

[14]J. E. Hirsch, B. A. Huberman, and D. J. Scalapino, Phys. Rev. A **25**, 519 (1982).